

# EVOLUTION OF MICROSTRUCTURE DURING HOT DEFORMATION OF INCONEL 625 ALLOY WITH DIFFERENT STRAIN RATES

Received – Priljeno: 2018-02-03

Accepted – Prihvačeno: 2018-08-20

Original Scientific Paper – Izvorni znanstveni rad

Hot compressions tests of Inconel 625 superalloy were conducted using a deformation dilatometer to the strain level of 0,7 at 1 050 °C, with a different strain rate. Optical microscope and electron backscatter diffraction technique were used to investigate the microstructure evolution and nucleation mechanisms of dynamic recrystallization. Microstructural evolution of Inconel 625, deformed to the strain level of 0,7 at 1 050 °C, reveals that the size of the dynamic recrystallization (DRX) grains and the fraction of DRX increase with the decrease in strain rate. At the strain rate 10 s<sup>-1</sup>, the grain sizes are mainly located in the size below 20 μm, indicating that nucleation of DRX was dominant due to the combined effects of high stored energy and short deformation time for grain growth at high strain rate.

*Key words:* Inconel 625, hot compression test, strain rates, microstructural evolution, grain size

## INTRODUCTION

Inconel nickel-chromium alloy 625 is used for its high strength and outstanding corrosion resistance. The strength of Inconel alloy is derived from the stiffening effect of molybdenum and niobium on its nickel-chromium matrix; thus precipitation-hardening treatments are not required. This combination of elements is also responsible for superior corrosion resistance to a wide range of corrosive environments of unusual severity as well as the high-temperature effects. During the hot deformation of metals or alloys, material flow behaviour is often very complex, and the control of microstructure is important to optimize the final mechanical properties [1]. Studies show that the work hardening (WH), dynamic recovery (DRV) and dynamic recrystallization (DRX) occur in the metals and alloys with low stacking fault energy during hot deformation [2,3]. Generally, DRX is not only an important softening mechanism, but also an effective method to refine size. The nickel-based superalloys are used in modern aero engines and gas turbine. The strengthening mechanism is mainly ascribed to the coherent  $\gamma'$  (L1<sub>2</sub> Structure with Ni<sub>3</sub>(Al,Ti) composition and  $\gamma''$  (DO<sub>22</sub> structure with Ni<sub>3</sub>Nb composition) phases in the face centered cubic matrix ( $\gamma$  phase) [4].

## EXPERIMENTAL

Flat specimens of Inconel 625, with chemical composition in Table 1, were used for hot-deformation tests. The specimens were cut from 11 mm thick hot-rolled plate. Cylindrical specimens with a diameter of 5 mm

and height of 10 mm were machined from flat specimens of Inconel 625. Hot compression tests were performed on a TA Instruments DIL805A/D. One temperature (1 050 °C) and four different strain rates (0,01, 0,1, 1 and 10 s<sup>-1</sup>) were used in the hot compression tests, and the final log. deformation degree was 0,7. Each specimen was heated to 1 050 °C at a heating rate of 10 °C/s and then soaked for 10 minutes. The stress-strain data were automatically recorded by the testing system during the hot compression. The specimens were immediately quenched by argon after each experiment. Then the deformed specimens were cut along the compression axis section for microstructural analysis. After polishing and ion etching the samples were observed by optical and scanning electron microscope.

Table 1 **Chemical composition of Inconel 625 /wt.%**

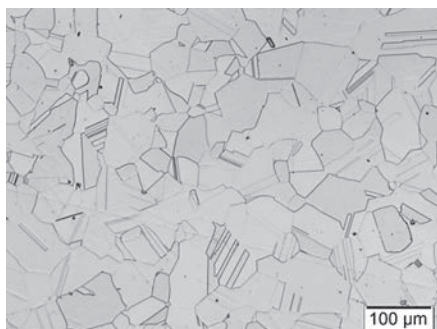
C	N	Ni	Mo	Nb	Cr	Ti
0,01	0,018	63,4	8,7	3,5	21,8	0,29

## RESULTS AND DISCUSSION

Figure 1 shows the initial microstructure of Inconel 625 before hot deformation. The specimens had a fine homogeneous  $\gamma$  phase with carbides solute in the matrix. The microstructure consists of equiaxed austenitic grains with a mean grain size of 80 μm and a large number of annealing twins, typical for alloys with low stacking fault energy [5].

Figure 2 shows the true stress-true strain curves of the alloy deformed a 0,7 true strain at 1 050 °C with different strain rates. Obviously, there is a work-hardening stage at the strain less than 0,2, which is mainly caused by the increase of dislocation density and the formation

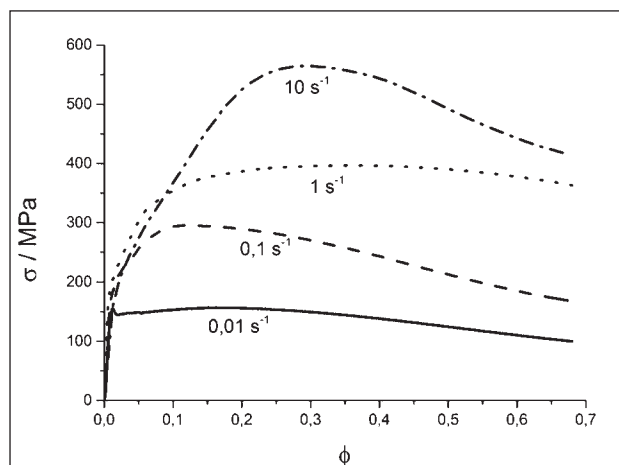
F. Tehovnik (e-mail: franc.tehovnik@imt.si), J. Burja, S. Malej, F. Vode, B. Podgornik, B. Arh, B. Šetina Batič, Institute of Metals and Technology, Ljubljana, Slovenia



**Figure 1** Optical micrograph of the studied superalloy before hot deformation

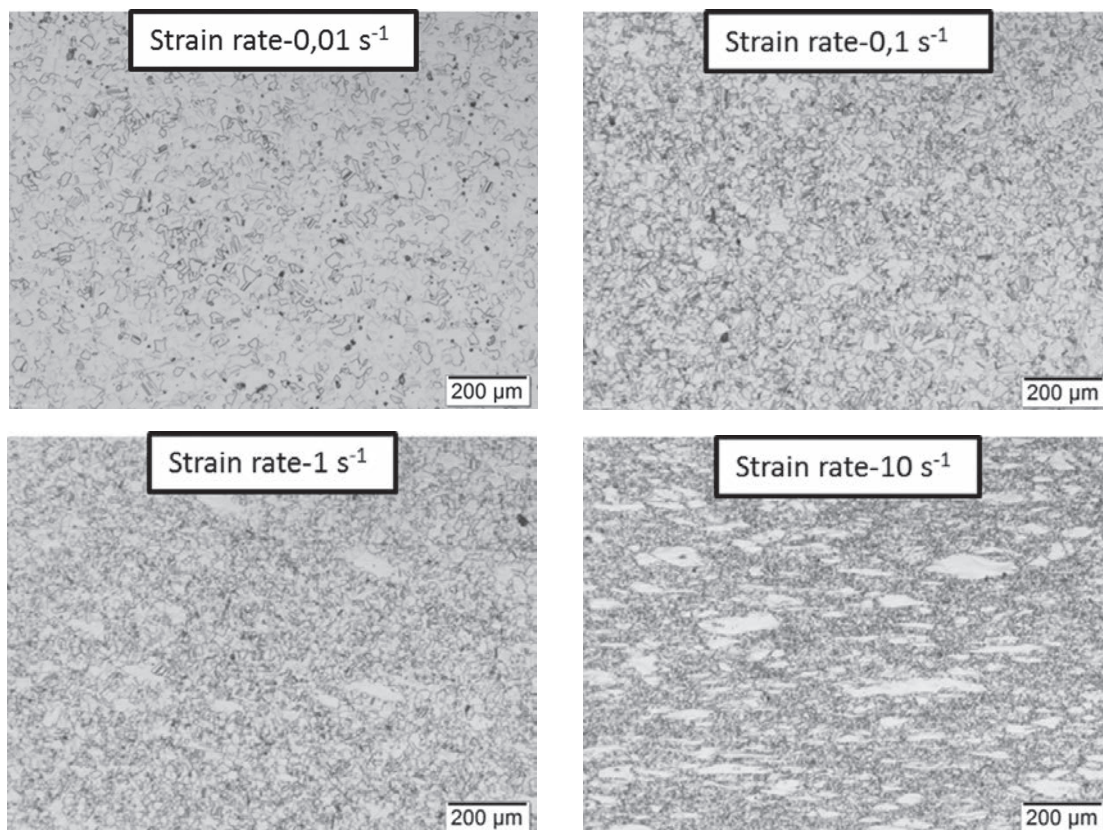
of poorly developed subgrain boundaries. With the increasing strain dynamic softening mechanisms occur, leading to the decrease of flow stress. In general the hot deformation is a competing process between the work hardening and dynamic softening. At the strain rate of  $1 \text{ s}^{-1}$  a steady-state flow stress can be reached. This means the work hardening and dynamic softening mechanisms reached a dynamic equilibrium. At the strain rate of  $10 \text{ s}^{-1}$  the curves exhibit continuous flow softening. Figure 2 shows that the flow stress is sensitive to the strain rate. At high strain rates, the reduction of deformation time restrains the growth of DRX grains and increases the work hardening effect. Thus, the flow stress at high strain rate is higher than at low strain rate [5-7].

Figure 3 shows the evolution of microstructure of the alloy deformed to the 0,7 true strain at  $1050 \text{ °C}$  with different strain rates. The nucleation and the growth of DRX grains, the volume fraction of DRX grains, and average



**Figure 2** True stress-true strain curves of the alloy deformed to a 0,7 true strain at  $1050 \text{ °C}$  with different strain rates

grain size are strongly influenced by the strain rate. At the strain rate  $10 \text{ s}^{-1}$  the microstructure is composed of elongated deformed grains and fine DRX grains (Figure 3, strain rate- $10 \text{ s}^{-1}$ ). At the strain rate of  $1 \text{ s}^{-1}$ , small DRX grains and some deformed grains are visible (Figure 3, strain rate  $1 \text{ s}^{-1}$ ). The new recrystallized grains nucleate on the deformed grain boundaries and form a necklace around it [8-10]. With the decreasing strain rate, the initial large grains disappeared and more DRX grains are formed (Figure 3, strain rate  $0,1 \text{ s}^{-1}$ ). The specimen deformed at the strain rate of  $0,01 \text{ s}^{-1}$  has a fully recrystallized microstructure, it is composed of uniform and small DRX grains (Figure 3, strain rate  $0,01 \text{ s}^{-1}$ ). This is very similar to the research of Zhang H. et al [11].



**Figure 3** The evolution of microstructure of the alloy deformed to a 0,7 true strain at  $1050 \text{ °C}$  with different strain rates

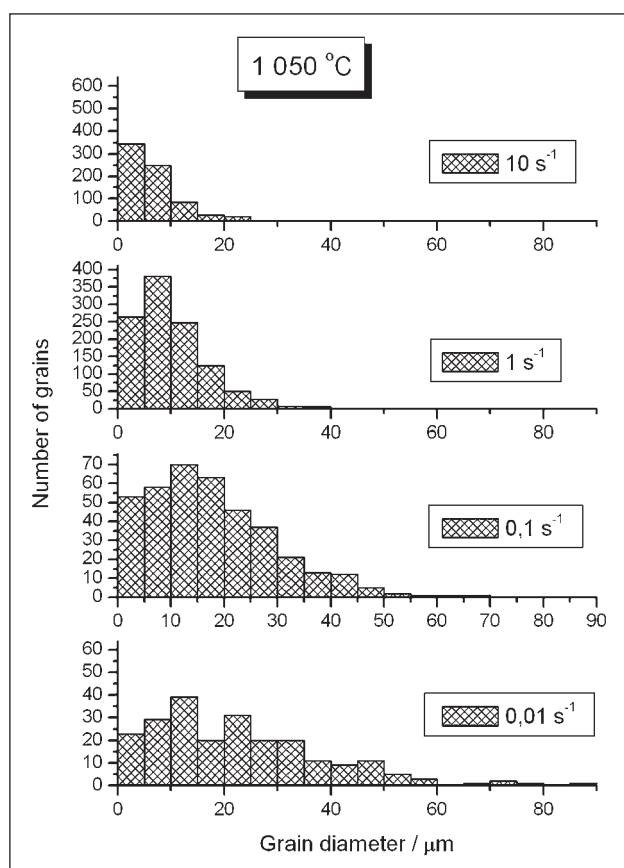


**Figure 4** Grain sizes distribution and number of grains of the alloy deformed at 1050 °C at different strain rates

The microstructural evolution of Inconel 625, deformed to the strain level of 0,7 at 1050 °C, reveals that the size of the DRX grains and the fraction of DRX increase with the decrease in strain rate.

Figure 4 shows the grains size distributions and number of grains of the alloy deformed at 1050 °C. At the strain rate 10 s<sup>-1</sup>, the grain size are mainly located in the size below 20 μm, indicating that nucleation of DRX was dominant due to the combined effects of high stored energy and short deformation time for grain growth at high strain rate. In their words, higher nucleation and lower growth during high strain rate deformation led to finer DRX grains.

The „deformation“ component illustrates the change of the crystal lattice orientation from point to point in each grain. Deviation from the average orientation of the grain (misorientation) is calculated for each grain. If this value exceeds the critical angle (usually defined between 1 and 2 degrees), the grain is deformed. Some grains are composed of subgrains, whose internal deviation from the mean orientation is smaller than the critical angle, and the deviation between the subgrains is greater than the critical angle - these grains are defined as substructured. All other grains are classified as recrystallized. In the strain rate range of 0,01-10 s<sup>-1</sup>, the volume fraction of DRX grains decreases with increasing strain rate. The lower strain rate can provide more time for grain boundary migration, which can promote the development of DRX process. With increasing

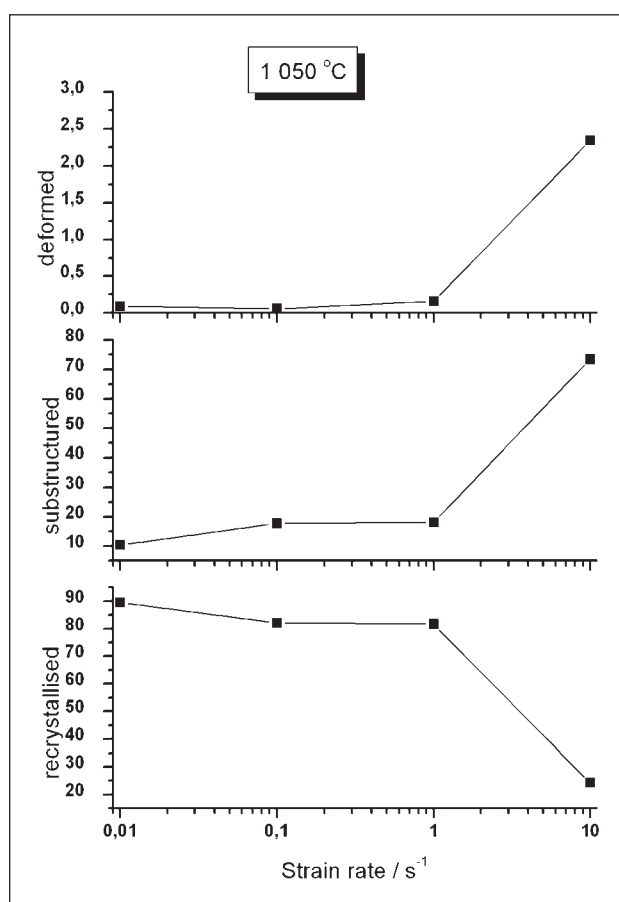


**Figure 5** The volume fractions of DRX grains at different strain rate

strain rate (10 s<sup>-1</sup>) many DRX grains and incomplete necklace structures appear (see Figure 5). The acceleration of DRX at the minimum strain rate results from the fact that the decrease in the critical dislocation density leads to a decline of the critical strain required for the initiation of DRX [6, 12].

## CONCLUSIONS

Hot compressions tests of Inconel 625 superalloy were conducted using a deformation dilatometer to the strain level of 0,7 at 1050 °C, with a different strain rates. The conclusions are as follows:

The flow stress is strain rate dependent and increases with increasing strain rate. The flow curves are characterized by the initial rapid work hardening stage to attain a peak stress at the a true strain of 0,2 followed by flow softening at the strain rate 10 s<sup>-1</sup>. At the lower strain rates a steady flow stress is observed in contrast to that observed at the higher strain rate, where stress decreases gradually.

Microstructural evolution of Inconel 625, deformed to the strain level of 0,7 at 1050 °C, reveals that the size of the DRX grains and the fraction of DRX increase with the decrease in strain rate.

At the deformation strain rate 0,01 s<sup>-1</sup> the specimen has fully recrystallized during hot deformation. Incomplete recrystallization occurs when deformed with the

strain rate  $10 \text{ s}^{-1}$ , the recrystallization begins at the deformed grain boundaries, being consistent with the necklace mechanism.

## REFERENCES

- [1] Lin Y. C, Chen X. M. A critical review of experimental results and constitutive descriptions for metals and alloys in hot working, *Mater. Des.* 32 (2011), 1733-1759
- [2] Lin Y. C, Chen M. S, Zhong J. Constitutive modelling for elevated temperature flow behaviour of 42CrMo steel, *Comp Mater Sci.* 42 (2008), 470-477
- [3] Chen F, Cui Z. S, Chen S. J. Recrystallization of 30Cr2Ni-4MoV ultra –super-critical rotor steel during hot deformation. Part 1: Dynamic recrystallization, *Mat. Sci. Eng. A* 528 (2011), 5073-5080
- [4] Nalawade S, Sundararaman M, Singh J. B, Verma A, Kishore R. Comparison of deformation induced precipitation behaviour in Alloy 718 under two microstructural conditions, *Trans. Indian Inst. Met.* 63 (2010), 35-41
- [5] Hoseini Asli A, Zarei-Hanzaki A. Dynamic recrystallization behaviour of a Fe-Cr-Ni super-austenitic stainless steel, *J. Mater. Sci. Technol.* 25 (2009), 603-606
- [6] Wang Y, Shao W. Z, Zhen L, Zhang X. M. Microstructure evolution during dynamic recrystallization of hot deformed superalloy 718, *Mat. Sci. Eng. A* 486 (2008), 321-332
- [7] Momeni A, Dehghani K. Microstructural Evolution and Flow Analysis during Hot Working of Fe-Ni-Cr Superaustenitic Stainless Steel, *Metall. Mater. Trans. A* 42 (2010), 1925-1932
- [8] Mirzadeh H, Najafizadeh A. Hot deformation and Dynamic Recrystallization of 17-4 PH Stainless Steel, *ISIJ Int.* 53 (2013) 4, 342-350
- [9] Tehovnik F, Žužek B, Arh B, Burja J, Podgornik B. Hot rolling of the superaustenitic stainless steel AISI 904L, *Materiali in Tehnologije* 48 (2014) 1, 137-140
- [10] Li D, Guo Q, Guo S, Peng H, Wu Z. The microstructure evolution and nucleation mechanisms of dynamic recrystallization in hot deformed Inconel 625 superalloy, *Materials & Design* 32 (2011) 2, 696-705
- [11] Zhang H, Zhang K, Zhou H, Lu Z, Zhao C, Yang X. Effects of strain rate on microstructure evolution of nickel-based superalloy during hot deformation, *Materials & Design* 80 (2015), 51-62
- [12] Field D, Bradford L, Nowell M, Lillo T. The role of annealing twins during recrystallization of Cu, *Acta Mater.* 55 (2007), 4233-4241

**Note:** Responsible person for English translation M. M. Travnik Vode, Višnja Gora, Slovenia